A maximally particle-hole asymmetric spectrum emanating from a semi-Dirac point

Yundi Quan and Warren E. Pickett
Department of Physics, University of California, Davis, CA 95616
(Dated: September 23, 2017)

Tight binding models have proven an effective means of revealing Dirac (massless) dispersion, flat bands (infinite mass), and intermediate cases such as the semi-Dirac (sD) dispersion. This approach is extended to a three band model that yields, with chosen parameters in a two-band limit, a closed line with maximally asymmetric particle-hole dispersion: infinite mass holes, zero mass particles. The model retains the sD points for a general set of parameters. Adjacent to this limiting case, hole Fermi surfaces are tiny and needle-like. A pair of large electron Fermi surfaces at low doping merge and collapse at half filling to a flat (zero energy) closed contour with infinite mass along the contour and enclosing no carriers on either side, while the hole Fermi surface has shrunk to a point at zero energy, also containing no carriers. The tight binding model is used to study several characteristics of the dispersion and density of states. The model inspired generalization of sD dispersion to a general $\pm\sqrt{k_x^{2n}+k_y^{2m}}$ form, for which analysis reveals that both n and m must be odd to provide a diabolical point with topological character. Evolution of the Hofstadter spectrum of this three band system with interband coupling strength is presented and discussed.

PACS numbers: 71.20.-b,73.43.Lp

I. BACKGROUND

Peculiarities in crystalline electronic spectra connected to anomalies in materials behavior, from topologically protected edge states of topological insulators[1–3] to quantum critical behavior in intermetallic compounds,[2,4] have brought discussion of unconventional crystalline band structures to the forefront of materials research. The massless Dirac band structure at the Fermi point of graphene and related physical systems have been well studied.[5,6] Graphene has Fermi points at the intrinsic chemical potential as do conventional zero-gap semiconductors,[7] but has linear dispersion corresponding to massless fermions appearing in Dirac theory and in two-component Weyl theory. Quadratic band touching has raised stimulating issues, as have flat bands whose eigenstates are strictly localized orbitals.[8]

Recently increased attention to the characterization of the spectra, and of degeneracies and their topological consequences, of Hamiltonians $H_k(\{\alpha\})$ has increased in activity in a number of respects since the early work of von Neumann and Wigner.[9] The crystal momentum k is a continuous wavevector in the Brillouin zone (BZ) – here it is two dimensional (2D) – and $\{\alpha\}$ represents the parameters that appear in the Bloch Hamiltonian. von Neumann and Wigner established that for general Hermitian Hamiltonians, three parameters are necessary and sufficient to produce degeneracy, while only two are required for real Hamiltonians. Especially since the production and intense study of graphene with its pair of Dirac points at the chemical potential, interest in these issues and the various phases that arise, viz. Dirac and Weyl points,[10,11] and nodal line semimetals,[12–15] has intensified.

A crystalline eigenvalue spectrum $E_{k,n}(\{\alpha\})$ may be classified in various ways, while the topological character of $h_k(\{\alpha\})$ can be determined from the eigensystem: $E_{k,n}(\{\alpha\})$ and the corresponding eigenfunctions $u_{k,n}(\{\alpha\})$. Particular interest centers on degeneracies of $E_{k,n}(\{\alpha\})$ and topological aspects of the electronic system, and their origins and functionalities. Topological character is directly related to non-analyticities arising from degeneracies,[16] as understood to some degree in the earlier days of gapless semiconductors.[7] Berry dubbed such points of degeneracy and non-analyticity diabolical points.[16] In many studies of the topological character of the system, the parameters of the Hamiltonian are simply the two components (three components) of the two dimensional [2D] (respectively, three dimensional [3D]) wavevector, thereby keeping the any other parameters in the Hamiltonian fixed.

In the class of touching bands, a unique intermediate case between conventional zero-gap semiconductors with quadratic touching and the linear Weyl (Dirac) spectrum, in two dimensions is provided by semi-Dirac (sD) dispersion; sD fermions are massless along one axis but massive in the perpendicular direction. sD dispersion in crystalline systems was first obtained by Hasegawa *et al.*[17] in a tuned anisotropic honeycomb model, with its properties elaborated by Montambaux and collaborators.[18–20] A sD spectrum was discovered in VO_2 nanolayers where tuning of the system was unnecessary: various parameters of the system could be varied while only the position of the sD point along a diagonal in the Brillouin zone would change,[21–24] being protected by space group symmetries. The dispersion was modeled with the low energy Hamiltonian and resulting dispersion E_k by

$$\begin{aligned} h_k &= \frac{k_x^2}{2m}\tau_x + vk_y\tau_y, \\ E_k &= \pm\sqrt{(\frac{k_x^2}{2m})^2 + (vk_y)^2}, \end{aligned} \tag{1}$$

m and v are the mass and velocity, and $\vec{\tau}$ is the vector of Pauli matrices in orbital space. sD behavior is excep-

tional; not only does it display extreme anisotropy, it also presents a case in which the kinetic energy operator in the effective Hamiltonian is non-relativistic $p^2/2m$ in one direction but has the relativistic vp form in the perpendicular direction. Generalizing this semi-Dirac behavior and obtaining additional anomalous behavior in the spectrum is a primary aspect of this paper.

At the other end of the spectrum of peculiar bands is the flat band case,[25–28] where at appropriate filling the "Fermi surface" corresponds to the entire Brillouin zone (or nearly so), which forms the extreme opposite limit from the Fermi points in the cases mentioned above. A completely flat band introduces a δ-function density of states (DOS), enabling instabilities of many kinds, of which ferromagnetism has attracted much study.[25] Areas or lines of flatness have less effect on the DOS but still important. Even points of flatness (van Hove singularities) can impact properties strongly.

How the unusual dispersion interplays magnetic fields, for example the Landau level structure, has been studied for the sD system.[18,22,24] The broader picture includes the effect on the Hofstadter spectrum[29] at arbitrary field strengths. For the sD case, Delplace and Montambaux presented results aimed primarily at experimental verification in cold atom systems.[20] The question how strong particle-hole asymmetry affects the Hofstadter spectrum has not, to our knowledge, been discussed in the sD context, and that is partial motivation for the present paper. Such studies have been extended to other model systems, including sD and related systems as well.[20,22,24,31] The Hofstadter spectrum for the strongly particle-hole asymmetric model of semi-Dirac system is addressed in this paper.

The manuscript is organized as follows. In Sec. II we present a straightforward generalization of the sD Hamiltonian to a class of Hamiltonians retaining sD points but having unusual spectra in certain regimes and limiting cases. We give special attention to a regime in which the *sD mass diverges*, at which point the model interpolates between zero to infinite mass with angle. For infinite mass, the sD points degenerate into a closed loop with flat energy at the band bottom. As a result, doping with small carrier density n away from half-filling produces *two large* Fermi surfaces enclosing the *small density* n of holes for electron doping, but opens conventional with highly anisotropic small Fermi surfaces for hole doping.

Degeneracies at crossing bands are known to be a source of topological character, viz. Berry phases. The non-topological character of the sD point was pointed out already by Dietl *et al.*[18] The topological versus trivial character of sD models was further studied and generalized by Huang *et al.*,[30] a topic to which we return in Sec. III.B. This inquiry into topological character at degeneracies arising from crossing bands is the topic of Sec. III.A, where results are given for general low energy dispersion of the form

$$E_k = \pm\sqrt{\alpha k_x^n + \beta k_y^m}, \tag{2}$$

where α, β are constants.

Sec. IV provides an extension of the study of Dietl *et al.* and later Delplace and Montambaux of the Hofstadter spectrum of the sD model.[18,20] Specifically, we illustrate the evolution of the Hofstadter butterfly spectrum of this asymmetric sD model as the strength of coupling of the two active bands to high lying band is increased. **Chern numbers.** A summary is provided in Sec. V.

II. 3-BAND MODEL; FOLDING TO 2-BANDS

The tight binding Hamiltonian used previously[22,24] to produce the sD electronic structure, corresponding to the t'=0 limit of the density of states shown in Fig. 1, was based on a three band model consisting of two uncoupled orbitals on a square lattice, with each coupled anisotropically to a distant (in energy) third band, with Hamiltonian (lattice constant a=1)

$$h_k = \begin{pmatrix} \varepsilon_{1k} & 0 & V_k \\ 0 & \varepsilon_{2k} & V_k \\ V_k & V_k & \varepsilon_3 \end{pmatrix}; \qquad h_k u_{nk} = E_{nk} u_{nk}, \tag{3}$$

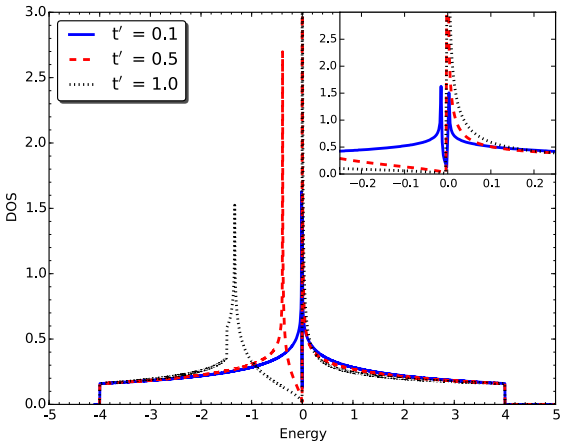

FIG. 1: The density of states (DOS, in arbitrary units) for the three cases of coupling λ = -0.002, -0.05 and -0.2 (black, dashed red, dashed black respectively), corresponding to the respective values of t' in the legend. The other parameters are Δ=0, $\bar{t}$ = 1, δ = 0. The inset illustrates the fine structure near zero energy (the band centers); blue corresponds to $\lambda = -0.002$. The breaking of particle-hope symmetry around zero energy is apparent.

Here we generalize the original sD tight binding model, so that orbitals 1 and 2 (also referred to as s and s') separately, with hopping amplitudes t_1 and t_2 respectively, give rise to a band that has studied extensively in the context of the high temperature superconducting cuprates, notably displaying a van Hove singularity at the zone corner. These two bands have bands have centers of gravity

differing by Δ and hopping amplitudes differing in magnitude by $\delta = t_2 - t_1$ from the mean value of $\bar{t}$, with associated differences in bandwidths:

$$\begin{aligned} \varepsilon_{1k} &= -\Delta/2 + 2t_1(\cos k_x + \cos k_y) \\ \varepsilon_{2k} &= +\Delta/2 - 2t_2(\cos k_x + \cos k_y) \\ V_k &= 2t'(\cos k_x - \cos k_y). \end{aligned} \tag{4}$$

Thus we have $t_1 = \bar{t} - \frac{\delta}{2}$, $t_2 = \bar{t} + \frac{\delta}{2}$. These two uncoupled bands each couple with amplitude t' to a high-lying band 3 at energy ε_3 and negligible dispersion. The anisotropic coupling with orbital 3 expressed in V_k can be realized for orbitals 1 and 2 with full site symmetry (viz. s or d_{z^2}) and orbital 3 of $d_{x^2-y^2}$ symmetry. The pertinent point is that this hybridization vanishes along the diagonals $k_y = \pm k_x$.

A. Uncoupled bands

For coupling t'=0, band 1 (respectively 2) has bandwidth $8t_1$ ($8t_2$) with a divergent van Hove singularity (vHs) at - $\Delta/2$ (+ $\Delta/2$), which will however not be our main concern. These bands cross (or in common usage, 'touch') at

$$\cos k_x + \cos k_y = \frac{\Delta}{4\bar{t}} = 2\frac{\Delta}{W} \equiv 2\gamma \tag{5}$$

where W is the mean bandwidth of bands 1 and 2. This relation describes a curve $\mathcal{C}_\gamma$ in the Brillouin zone (BZ) given parametrically by

$$k_y = \pm \cos^{-1}(2\gamma - \cos k_x), \tag{6}$$

whenever a real solution exists. The bands are both *degenerate* and *constant* (flat) over this Fermi curve $\mathcal{C}_\gamma$, with energy

$$E_\gamma = -2\delta\frac{\Delta}{W} = -2\delta\gamma, \tag{7}$$

which differs from zero only if *both* δ and Δ are non-zero, *i.e.* both the band centers and the band widths differ.

This closed line of degeneracies is an example of a nodal loop semimetallic electronic structure.[12–15] With generic coupling such degeneracies are normally lifted to anticrossings, but Herring demonstrated that such nodal loop degeneracies can occur purely accidentally (independent of symmetry restrictions) and several examples have recently been reported, see for example the list of references given by Xu *et al.*[32]. We will return to this point.

In the limit $\Delta \to 0$ ($\gamma \to 0$) of equal band centers this uncoupled system has two coinciding diamond shaped Fermi surfaces (the shape familiar from 2D square lattice models) at half filling of both bands, and a coalescing of the van Hove singularities at $\Delta = 0$. Without coupling, the density of states (DOS) remains the sum of that from the two square lattice DOSs with well known shapes. At γ=1 the DOS curves just touch, giving a gapless semiconductor. For larger γ a gap opens between the bands. $\gamma > 1$ does not interest us here.

B. Adding the coupling

We consider ε_3 large compared to W and Δ so that band 3 lies at high energy and can be neglected once the coupling is taken into account. Figure 1 illustrates the very strong particle-hole asymmetry around the energy zero induced by the coupling. The vHs splits roughly symmetrically for very small coupling (blue curve). However, for still small coupling $\lambda = -0.05$, the asymmetry is substantial: the lower vHs is shifted downward where the upper one remains very close to zero. The asymmetry becomes ever clearer for increasing λ. Regardless of the size of λ however, band touching at zero energy remains. The strongly differing slopes of the DOS at positive and negative energy reflects the different masses.

When t' is of the same order as, or smaller than, $\bar{t}$, the three-band model can be downfolded into a two band model by treating band 3 perturbatively, giving

$$h_k = \begin{pmatrix} \epsilon_{1k} + \lambda_k & \lambda_k \\ \lambda_k & \epsilon_{2k} + \lambda_k \end{pmatrix} \tag{8}$$

The downfolded bands (still called band 1 and 2) continue to touch at one point along the diagonals, which provides the sD point discovered in the thin heterostructure system $VO_2/TiO_2(001)$.[21,23] Along the contour $\mathcal{C}_\gamma$ the coupling λ_k separates the bands everywhere except along the diagonals where it vanishes. The relation for λ_k is

$$\lambda_k = \lambda(\cos k_x - \cos k_y)^2 : \quad \lambda \equiv -4\frac{t'^2}{\epsilon_3}. \tag{9}$$

The sD points of touching bands $\lambda_k = 0$ occur at $(\pm k_c, \pm k_c)$ with k_c=$\cos^{-1}\gamma$. Note that the difference in bandwidths given by $\delta \neq 0$ does not enter this condition; only the ratio of band center difference Δ and mean bandwidth W enters, so this condition is not unusually sensitive to details of the bands. The two band Hamiltonian becomes

$$\begin{aligned} H_k &= h_o(k)\tau_0 + \vec{h}(k)\cdot\vec{\tau} \\ &\to \bar{\varepsilon}_k\tau_0 + \lambda_k\tau_1 + \Delta_k\tau_3 \end{aligned} \tag{10}$$

in terms of Pauli matrices τ_j in orbital space, the mean band energy $\bar{\varepsilon}_k$ and half-separation Δ_k are

$$\bar{\varepsilon}_k = -\delta(\cos k_x + \cos k_y) + \lambda_k, \tag{11}$$

$$\Delta_k = -\frac{\Delta}{2} + 2\bar{t}(\cos k_x + \cos k_y). \tag{12}$$

The separation of two bands is given quite generically by twice the magnitude of $\vec{h}_k$:

$$\begin{aligned} E_{k\pm} &= h_0(k) \pm |\vec{h}(k)| \\ &\to \bar{\varepsilon}_k \pm \sqrt{\lambda_k^2 + \Delta_k^2}. \end{aligned} \tag{13}$$

Since H_k is real the Berry connection (hence Berry curvature, vanishes, so topological character is absent,

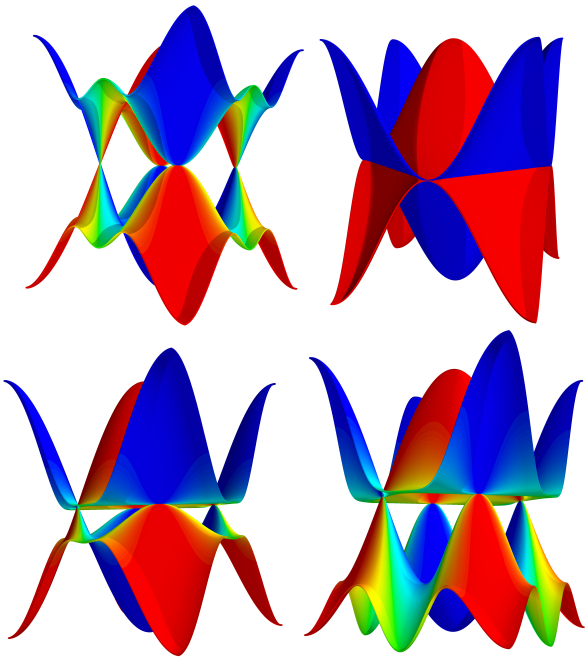

FIG. 2: (Color online) Top row: particle-hole symmetric dispersions plotted across the square Brillouin zone. Top left: schematic representation of particle-hole symmetric semi-Dirac dispersion. Top right: dispersion of uncoupled two band model. Bottom row: particle-hole asymmetric two band model driven by s (s') and d interaction. Bottom left: $\bar{t}=1$, $\delta=0$, $\Delta=0$, $t'=1$, $\epsilon_d=30$. Bottom right: $\bar{t}=1$, $\delta=0$, $\Delta=0$, $t'=2$, $\epsilon_d=30$. Note the strong shift of the lower band downward.

as observed earlier.[18] Our interest is the eigenvalue spectrum and energy surface topology of the coupled bands. We study specifically the lowest two bands, which we refer to as the particle-hole asymmetric two band model (a2BM). Figure 1 illustrates the DOS when the uncoupled bands are degenerate $\Delta=0=\delta$, versus coupling strength t'. The initially coinciding vHs separate, with one remaining very nearly at zero energy (the bottom of band 2), thereby assuming the single-sided divergence characteristic of one dimensional systems. We return to the corresponding diverging effective mass below.

C. Band dispersion

This band topology, shown in Fig. 2 for a select set of parameters, differs in striking ways from other unusual cases, and from the closely related sD form discussed previously.[22] The bands always touch at the critical point $(\pm k_c, \pm k_c)$ along the diagonal given by

$$\cos k_c = \gamma. \tag{14}$$

Only for band center separation Δ=0, the critical point lies at $(\frac{\pi}{2}, \frac{\pi}{2})$, otherwise its position is determined by the value of Δ. Expanding the dispersion near the semi-Dirac point and rotating by $\frac{\pi}{4}$ from k_x, k_y to q_1, q_2 yields

$$E_\pm = E_\gamma + \sqrt{2}\delta\sqrt{1-\gamma^2}q_2 + \left[\tfrac{1}{2}\delta\gamma + 2\lambda(1-\gamma^2)\right]q_1^2 \pm \sqrt{8\bar{t}^2q_2^2(1-\gamma^2) + \left[4\lambda^2(\gamma^2-1)^2 + \bar{t}^2\gamma^2\right]q_1^4}$$

Along the $q_1=0$ axis (the original diagonal) the dispersion reduces to linear in q_2

$$\begin{aligned} E_\pm &= E_\gamma + vq_2 \\ &= E_\gamma + 2\sqrt{2}(\frac{\delta}{2} \pm \bar{t})(\sin k_c)q_2 \end{aligned} \tag{15}$$

The dispersion in the perpendicular direction is quadratic in q_1

$$E_\pm = E_\gamma + \frac{q_1^2}{2m_\pm} \tag{16}$$

with effective masses given by

$$\frac{1}{2m_\pm} = \frac{1}{2}\delta\gamma + 2\lambda(1-\gamma^2) \pm \sqrt{4\lambda^2(\gamma^2-1)^2 + \bar{t}^2\gamma^2} \tag{17}$$

Aspects of this spectrum are discussed in the following subsections.

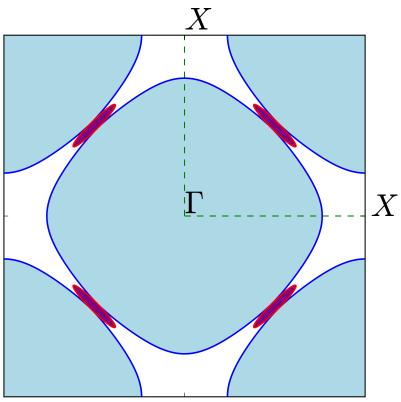

FIG. 3: (Color online) Iso-energy lines for small doping levels $\varepsilon = \pm 0.2$ (blue/red respectively). Electron doping leads to large Fermi contours around *both* Γ and corner M with carriers in the white areas, while hole doping leads to tiny, strongly distorted but non-elliptical contours (purple) enclosing the holes.

D. The case of Δ=0

For equal band centers $\Delta=0$ for which also $\cos k_c$=0 ($k_c = \frac{\pi}{2}$, γ=0), the mass m_- of the upper band 2 diverges, presumably leaving a much weaker dispersion, say q_1^4. The actual situation is more subtle than that.

For $\Delta = 0$, Cauchy's interlacing theorem[33] provides a general result. Given the coupled bands $E_{j,k}$ and uncoupled bands $\varepsilon_{j,k}$, the interlacing theorem states that coupled bands interlace the uncoupled bands, giving

$$E_{1k} \leq \varepsilon_{1k} \leq E_{2k} \leq \varepsilon_{2k} \leq E_{3k}. \tag{18}$$

Since $\varepsilon_{1k} = \varepsilon_{2k}$ are degenerate along C_γ, and furthermore are flat in energy at $E = E_\gamma$, along the entire contour $\mathcal{C}_\gamma$ given by Eq. 6, the bottom of the band (E_{2k}) is pinned at the band crossing energy E_γ along $\mathcal{C}_\gamma$. E_{k2} includes a flat contour which (numerical solutions verify) lies at the bottom of band 2, touching band 1 at the sD point. The resulting non-analyticity (a flat contour along a closed loop) is a more general one than that for Berry's isolated diabolical point.[16] $\mathcal{C}_\gamma$ comprises a closed line of points with massless dispersion in one direction and infinite mass in the other direction. This case is the one pictured in the lower panels of Figure 2.

This result just presented guarantees then that there is a constant energy contour that is the Fermi contour of band 2 at half filling, which at Δ=0 is the diamond-shaped Fermi contour of the single band tight-binding square lattice (TBSL) model at half filling. The similarity ends there, but it is instructive to contrast the evolution of the a2BM with the TBSL model as they are doped away from half filling. In the TBSL model, there is a symmetry, with identical electron and hole Fermi surfaces except the large hole surface is centered at Γ while the large electron surface is centered at M.

On the other hand, the a2BM is extremely particle-hole asymmetric. For slight electron-doping there are *two large, closed, Fermi contours* that are essentially the same as both electron and hole surfaces of the TBSL model. The electron carriers reside *between* these two large surfaces, as pictured in Fig. 3. At half filling the Fermi contours coalesce into a single Fermi contour with diamond shape connecting X points, before vanishing. Proceeding on to hole doping, tiny and highly anisotropic hole-like Fermi contours appear, centered on the $(\pm k_c, \pm k_c)$ sD points on the diagonals, with major axis oriented perpendicular to the diagonal, as illustrated in Fig. 3 and evident from Fig. 2. Thermal excitation at half filling will produce electron and hole carriers with vastly different behaviors, *i.e.* strong particle-hole asymmetry.

E. Effective mass and velocity at the semi-Dirac point

The on-site energy separation Δ, hopping integrals $\bar{t} \pm \frac{\delta}{2}$, or other parameters can be tuned by applying pressure or stress, providing a broad parameter space to design materials with distinctive behaviors. Here the dependence of effective masses and effective velocities of the tunable parameters will be discussed briefly. Recall that the average hopping parameter $\bar{t} = 1$ sets the energy scale. The effective velocities are given by

$$v_\pm = 2\sqrt{2}(1 \pm \frac{\delta}{2})\sqrt{1 - \frac{\Delta^2}{64}} \tag{19}$$

A difference in bandwidths δ makes the velocities differ, while a difference in band centers Δ affects the magnitudes. Applying pressure would broaden the band width and lift the limit of effective velocities to higher values.

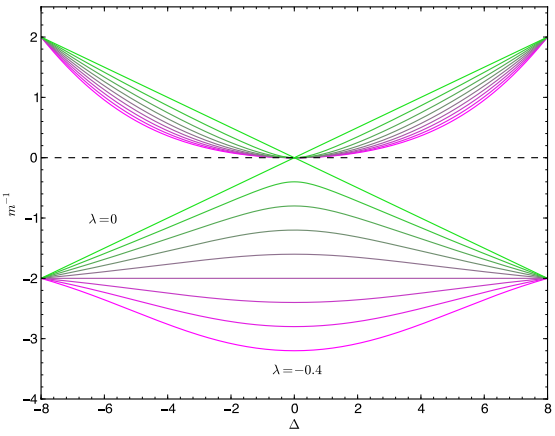

FIG. 4: Inverse of effective masses $m_\pm^{-1}$ versus on-site energy difference Δ. The band coupling λ is varied in increments of 0.05 from -0.4 to 0. When $\lambda = 0$, the inverse effective mass of upper and lower band become zero (effective mass diverges). As λ increases in magnitude, the upper band retains the infinite mass at $\Delta = 0$, while the effective mass of the lower band lowers rapidly to conventional values.

In Fig. 4 the inverse effective mass is plotted against on-site energy difference for a sequence of coupling strengths ($\lambda = -0.4, -0.35, ..., 0$) with $\delta = 0$. The on-site energy difference is varied from -8 to 8 (i.e. γ ranges from -1 to 1). In the absence of coupling where particle-hole symmetry is preserved, the effective mass varies linearly with the inverse of on-site energy difference Δ but diverges when the two orbitals near the Fermi level have identical on-site energy. As the magnitude of the coupling λ increases, the effective mass of the upper band remains infinite when $\Delta = 0$ (a flat contour), while the lower band has finite and decreasing effective mass. Interestingly, when the coupling reaches the special valuer $\lambda = -0.25$, m^{-1} for the lower band is independent of on-site energy separation of the s and s' orbitals.

III. TOPOLOGICAL ASPECTS FOR GENERALIZED DISPERSION

Topological character of electronic systems arises from the non-analyticity of the eigensystem occurring at degeneracies at points designated by Berry as diabolical points.[16] The occurrence or type of topological character is connected to the dispersion around the diabolical

point, viz. Dirac versus semi-Dirac versus conventional zero-gap, quadratic dispersion. The interest in sD systems arises from the qualitatively different electronic dispersion and resulting interpretation, viz. massive versus massless, which exhausts possibilities up to quadratic. Some results about the topological character of more general asymmetric Hamiltonians can however be derived.

A. Low energy region

A class of effective 2D Hamiltonians expanded around a band touching point can be written in terms of scaled dimensionless wavevectors as

$$h = \begin{pmatrix} 0 & k_x^m - ik_y^n \\ k_x^m + ik_y^n & 0 \end{pmatrix} = k_x^m \tau_x + k_y^n \tau_y \qquad (20)$$

m and n are integers. semi-Dirac dispersion is simply a special case with $m = 1$ and $n = 2$. The above effective Hamiltonian has two eigenvalues $\pm\sqrt{k_x^{2m} + k_y^{2n}}$. The corresponding eigenvectors can be written

$$u_\pm = \frac{1}{\sqrt{2}} \begin{pmatrix} \pm 1 \\ \frac{k_x^m + ik_y^n}{\sqrt{k_x^{2m}+k_y^{2n}}} \end{pmatrix} = \frac{1}{\sqrt{2}} \begin{pmatrix} \pm 1 \\ e^{i\theta_k} \end{pmatrix} \qquad (21)$$

where $\theta_k = tan^{-1}(k_y^n/k_x^m)$. The Berry connection under this gauge is

$$\vec{A} = i \langle u_\pm | \nabla | u_\pm \rangle = \pm \frac{1}{2} \frac{k_x^{m-1} k_y^{n-1}}{k_x^{2m} + k_y^{2n}} (mk_y, -nk_x) \qquad (22)$$

Integrating the Berry connection along an adiabatic loop around the origin $\mathcal{C}$: $k_x^{2m} + k_y^{2n} = C^2$, where C is a non-zero constant, gives

$$\begin{aligned} \beta &= \int_{\mathcal{C}} [A_x dk_x + A_y dk_y] \qquad (23) \\ &= \frac{\pi}{8}[(-2 + (-1)^m + (-1)^n) - (-1 + (-1)^n)(-1)^m \\ &\quad -(-1 + (-1)^m)(-1)^n] \\ &= -\frac{\pi}{4}[1 - (-1)^n][1 - (-1)^m]. \end{aligned}$$

β is non-zero (equal to -π) only when both m and n are odd.

Thus a semi-Dirac point $m = 1, n = 2$ *represented by this Hamiltonian* is, as pointed out earlier,[19,22] topologically trivial, unlike the conical Dirac point with $m = 1 = n$ in graphene.

B. Effect of symmetry lowering

The original picture of a semi-Dirac spectrum[21,22] is that it can be represented by a family of effective Hamiltonians $h = \vec{d_k} \cdot \sigma$ with the restriction that at small $|\vec{k}|$ the eigenvalues are $\pm|\vec{d_k}| = \pm\sqrt{k_x^2 + k_y^4}$. Huang *et al.*[30] have noted that direct numerical evaluation of the density functional Berry curvature and its integral in the original semi-Dirac material (a thin film of VO_2[21,22]) leads to a Chern insulating designation, rather than the expected trivial phase, when spin-orbit coupling opens a gap. They resolved this apparent contradiction as follows. Suppose that "semi-Dirac" dispersion is defined in a less restricted manner, that $\varepsilon_k = \pm k_y^2$ for k_x=0 and $\varepsilon_k = \pm k_x$ for k_y=0, rather than specifically as $\sqrt{k_x^2 + k_y^4}$, and thereby allowing for lower symmetry terms away from the diagonals. Then their non-intuitive choice (in our scaled variables)

$$\begin{aligned} d_x &= k_x - k_y^2; \quad d_y = \Gamma k_x k_y, \qquad (24) \\ \varepsilon_k &= \pm\sqrt{k_x^2 - 2k_x k_y^2 + k_y^4 + \Gamma^2 k_x^2 k_y^2} \end{aligned}$$

reproduces qualitatively the topological nature of this spectrum. Note that the rectangular symmetry has been broken: $k_x \leftrightarrow -k_x$ is no longer a symmetry; there are other choices for lowering the symmetry. In the VO_2 thin film, a slice of the rutile structure, Γ is quite small but non-zero. This example illustrates the feature that topological nature is a property of the eigensystem, and not of the spectrum alone.

C. Generalized Hamiltonian

We extend the above discussion to a general effective Hamiltonian

$$h(k_x, k_y) = f(k_x, k_y)\sigma_x + g(k_x, k_y)\sigma_y \qquad (25)$$

with the restriction that $f(k_x, k_y)$ and $g(k_x, k_y)$ have well defined parity with respect to mirroring each of k_x and k_y, given that the degeneracy (diabolical) point is at (0,0). In essence this requires rectangular mm symmetry. To simplify the discussion, we use the notation $(\pm\pm;\pm\pm)$ to identify the parity of f and g with respect to k_x, then with respect to k_y. For example, (-+;-+) means that $f(-k_x, k_y) = -f(k_x, k_y)$ and $f(k_x, -k_y) = f(k_x, k_y)$ and similarly for $g(k_x, k_y)$ for the last two eigenvalues. The Berry connection for the effective Hamiltonian is

$$\begin{aligned} A_x &= -\frac{1}{2} \frac{-g(k_x, k_y) f_x(k_x, k_y) + f(k_x, k_y) g_x(k_x, k_y)}{f^2(k_x, k_y) + g^2(k_x, k_y)} \\ A_y &= -\frac{1}{2} \frac{-g(k_x, k_y) f_y(k_x, k_y) + f(k_x, k_y) g_y(k_x, k_y)}{f^2(k_x, k_y) + g^2(k_x, k_y)} \end{aligned}$$

where $f_x = \partial f/\partial k_x$, etc. To have topological character, the integration of the Berry connection along a loop around the point (0,0) must be non-zero.

The following integration path will be used $(k_x^0, -k_y^0) \rightarrow (k_x^0, k_y^0) \rightarrow (-k_x^0, k_y^0) \rightarrow (-k_x^0, -k_y^0) \rightarrow (k_x^0, -k_y^0)$. Denote the integration along the four segments as I_i, i=1,2,3,4. Here, we write $I_1 + I_3$ explicitly,

$$I_1 + I_3 = -\frac{1}{2}\int_{-k_y^0}^{k_y^0} \frac{-g(k_x^0,k_y)f_y(k_x^0,k_y) + f(k_x^0,k_y)g_y(k_x^0,k_y)}{f^2(k_x^0,k_y)+g^2(k_x^0,k_y)} - \frac{-g(-k_x^0,k_y)f_y(-k_x^0,k_y) + f(-k_x^0,k_y)g_y(-k_x^0,k_y)}{f^2(-k_x^0,k_y)+g^2(-k_x^0,k_y)}]dk_y$$

The integral $I_2 + I_4$ has a similar form. Parity analysis of the above integration for the sixteen possible cases $(\pm\pm;\pm\pm)$ leaves only four cases with possible non-zero Berry phase, viz. $(+-;-+)$, $(++;--)$, $(-+;+-)$, and $(--;++)$. The sD case of the Huang *et al.*[30] representation is a more general one that corresponds to the lower symmetry imposed by a non-rectangular-symmetry imposed by the structure of the VO_2 thin film, thus does not fit into this classification.

IV. HOFSTADTER SPECTRUM OF THE GENERALIZED SEMI-DIRAC SYSTEM

The Hofstadter butterfly spectrum,[29] which illustrates the intricate and fractal structure of the energy spectrum versus (the fractional part of) the magnetic flux inside a unit cell for a 2D square lattice under magnetic field, has been attracting renewed attention. This interest and the rich behavior of the extended sD model has motivated us to study its spectrum under magnetic field. Delplace and Montambaux studied a tight binding model[20] with staggered on-site potential in which semi-Dirac points can be created, at one-half flux quanta per unit cell, through merging of two Dirac points by varying the on-site potential. We return to this work below to contrast it with our study. The Hofstadter spectrum of a honeycomb lattice in which variation of the second neighbor hopping amplitude makes the two Dirac points merge into a sD point was studied by Dietl *et al.*[18]

In this section, we first provide Harper's equations for the three-band model, and then discuss the impact of $s-d$ and $s'-d$ coupling on the spectrum of three-band semi-Dirac model under magnetic field.

A. Harper's equation for semi-Dirac system

For a 2D lattice under external magnetic field B with Landau gauge $\vec{A} = (0, Bx)$, the semi-Dirac tight-binding Hamiltonian after Peierls substitution can be written as

$$\begin{aligned} h = & \sum_{\alpha=1,m,n,\pm}^{3} [\epsilon_\alpha n_{mn,\alpha} \\ & + t_\alpha (c^\dagger_{mn} c_{m\pm 1 n\alpha} + c^\dagger_{mn} c_{mn\pm 1\alpha} e^{\mp i 2\pi m\phi})] \\ & + t' \sum_{mn,\pm} (c^\dagger_{mn,1} c_{m\pm 1 n,3} - c^\dagger_{mn,1} c_{mn\pm 1,3} e^{\mp i 2\pi m\phi} + h.c.) \\ & + t' \sum_{mn,\pm} (c^\dagger_{mn,2} c_{m\pm 1 n,3} - c^\dagger_{mn,2} c_{mn\pm 1,3} e^{\mp i 2\pi m\phi} + h.c.). \end{aligned}$$

Here (m,n) are the site indices along the x, y directions, respectively, and α sums over orbitals s, s' and d. ϕ is the flux threading the unit cell in units of the flux quantum ϕ_o. The generalized Bloch function $u_{m,n,\alpha}(\vec{k})$ at site (m,n) should satisfy

$$\begin{aligned} \epsilon u_{ms} &= \epsilon_s u_{ms} + t_s[u_{(m+1)s} + u_{(m-1)s} \\ &+ 2u_{ms}\cos(k_y - m\phi)] + t'[u_{(m+1),d} \\ &+ u_{(m-1),d} - 2u_{m,d}\cos(k_y - m\phi)] \end{aligned} \quad (26)$$

$$\begin{aligned} \epsilon u_{ms'} &= \epsilon_{s'} u_{ms'} + t_{s'}[u_{(m+1)s'} + u_{(m-1)s'} \\ &+ 2u_{ms'}\cos(k_y - m\phi)] + t'[u_{(m+1)d} \\ &+ u_{(m-1)d} - 2u_{md}\cos(k_y - m\phi)] \end{aligned} \quad (27)$$

$$\begin{aligned} \epsilon u_{md} &= \epsilon_d u_{md} + t'[u_{(m+1)s} + u_{(m-1)s} \\ &- 2u_{ms}\cos(k_y - m\phi)] + t'[u_{(m+1)s'} \\ &+ u_{(m-1)s'} - 2u_{ms'}\cos(k_y - m\phi)] \end{aligned} \quad (28)$$

Equations (26)-(28) are the Harper's equations for the three-band semi-Dirac model. In the uncoupled limit $t' = 0$, the matrix form of Eqs. (26)-(28) is block diagonal, with three non-zero blocks corresponding to s, s' and d respectively. The spectrum is simply the regular Hofstadter spectrum with well defined Chern number at each gap satisfying the Diophantine equation.

In the strong hybridization regime $t'/t \to \infty$, u_s and $u_{s'}$ depend solely on u_d. Then Eqs. (26)-(28) can be reduced to

$$\epsilon u_{ms} = t'[u_{(m+1),d} + u_{(m-1),d} - 2u_{m,d}\cos(k_y - m\phi)] \quad (29)$$

$$\epsilon u_{md} = 2t'[u_{(m+1)s} + u_{(m-1)s} - 2u_{ms}\cos(k_y - m\phi)] \quad (30)$$

A solution to the equations above is to have $u_{md} = \pm\sqrt{2}u_{ms}$, which leads to the 1D Harper's equation:

$$\epsilon u_{md} = \sqrt{2}t'_{\pm}[u_{(m+1)d} + u_{(m-1)d} - 2u_{md}\cos(k_y - m\phi)],$$

$\pm$ corresponds $u_{md} = \pm\sqrt{2}u_{ms}$ respectively.

In Fig. 5 the numerical solutions for different values of coupling t' are plotted. In the top three panels of Fig. 5 the spectra for the two bands near zero are plotted, while the spectrum of three-bands are plotted in lower three panels. This choice allows the revealing parts of the spectrum to be surveyed.

$t' = 0$. In this limit the decoupled s and s' orbitals provide conventional particle-hole symmetric Hofstadter spectra, shown in the upper left panel of Fig. 5.

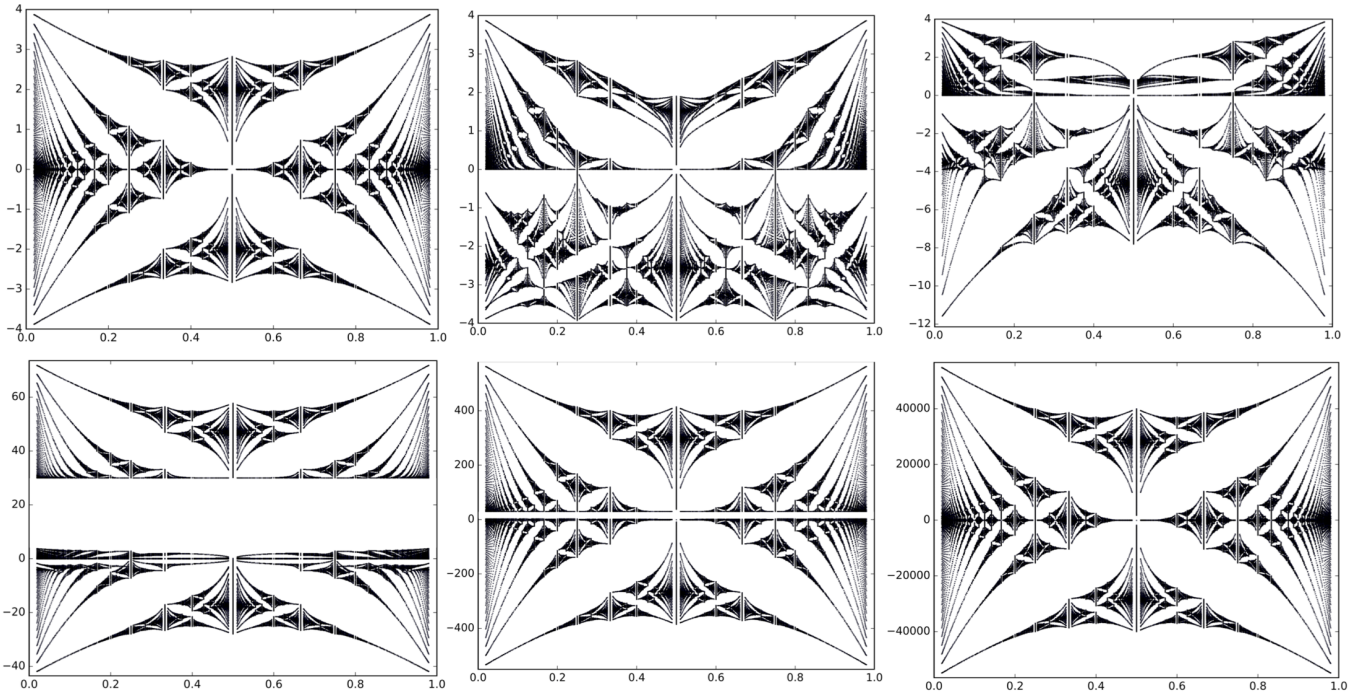

FIG. 5: Hofstadter-type display of the spectrum ϵ_k versus the relative magnetic flux ϕ/ϕ_0. From top left to bottom right: t' =0, 2, 4, 10, 100, 100000. In the top three panels only the two lower bands are shown, while in the lower three panels all three bands are displayed. Note the change in absolute scale from panel to panel.

$t' = 2$. This coupling strength is already large in absolute terms, but the energy separation $\varepsilon = 30$ makes the effective coupling $\lambda = 8/15$. As t' increases, the corresponding spectrum in Fig. 5 (upper middle panel) below zero (band 1) deforms smoothly but severely. The positive energy spectrum undergoes less severe change of compression downward, again reflecting the strong particle-hole asymmetry. Coupling to the third band opens a gap at zero energy except at $\alpha = 0$ (and probably $\alpha = 1/2$), where gapless character remains due to the vanishing of coupling along the diagonals of the zone. The bottom of the band 2 spectrum is flat and lies at zero. The spectrum of band 1 extends to nearer the bottom of the band, which is still at $E = -4$, for all values of the flux.

$t' = 4$. For this case ($\lambda \approx 2$) the spectrum has changed substantially. Band touching at $\alpha = 1/2$ and $1/4$ remains, as well as at no field. We note here that the spectrum has not been obtained very near several rational values of α because the denominator q in $p/q = \phi/\phi_0$ leads to progressively more substantial numerical work. Thus gapless versus small gapfull character is not clear from the figure. The positive energy band 2 has been compressed further downward, especially near $\alpha = 1/2$. Band 1 has been extended down to $E = -12$; gapless points remain at $\alpha = 0, 1/4$, and $1/2$.

$t' = 10$. The corresponding panel (lower left) for this case $\lambda \approx 13$ now includes band 3 and extends from $-50 < E < 75$. Band 2 is visible only as a strip of states in the $0 < E < 4$ range. The other interesting feature that emerges is that the spectrum of band 3 and band 1 are becoming symmetric around the midpoint of the large gap separating them.

$t' = 100$. On the scale of the spectrum now, $-500 < E < 500$, the band 2 spectrum is flat essentially at zero. The spectra of bands 1 and 3 dominate the figure and are nearly symmetric around $E = 0$.

$t' = 10^5$. This case is included to indicate that the spectrum essentially returns to the $t' = 0$ except for the very large change in energy scale. Band 2 remains compressed to very near zero energy. In this limit the band compressed to (effectively) zero is the antibonding combination of the original bands 1 and 2. The bonding combination of bands 1 and 2 form bonding and antibonding bands with the original band 3; these are the bands that form the butterfly in this limit.

An analogous progression of Hofstadter spectrum with variation of model parameter on a square lattice was reported by Delplace and Montambaux.[20] Their underlying square lattice was converted to a two-band system by applying an alternating on-site potential $\pm w$ along the $\hat{x}$ direction. The parameter that they varied was the magnitude of w, due to their observation that at the critical value of $w = 2t$ two Dirac points coalesce into a sD point. Their starting Hofstadter spectrum is the same as ours. Their model however retains particle-hole symmetry so the progression with strength of w cannot be compared with the progression of our spectrum with t'.

B. Chern number for semi-Dirac Hofstadter spectrum

Here we briefly note that Chern numbers can be obtained straightforwardly for the butterfly gaps. In a seminal paper by Thouless and coworkers (TKNN)[34] the total Hall conductance σ_{xy} for a 2D electronic system in a periodic potential and an external magnetic field was shown to be proportional to the integral of the Berry curvature of the occupied bands. For a strong periodic potential, the spectrum at $\phi/\phi_o = p/q \equiv \alpha$ (p and q are relatively prime integers) splits into q sub-bands with each band carrying an integer value of Hall conductance which can be found by solving a Diophantine equation. Goldman discussed the sequence of Chern numbers that characterize the square lattice Hofstadter butterfly[35] and compared with the honeycomb lattice spectrum. Rules to determine the Chern number at all scales of the Hofstadter spectrum were presented by Naumis and Satija.[36]

The Diophantine equation cannot be applied to the three-band model due to band crossings, but the Chern numbers for the three-band model under an external magnetic field perpendicular to the lattice can be calculated numerically. The Chern number for an isolated band or a band complex can be obtained either by integrating the Berry curvature over the entire Brillouin zone or by summing up the link variables on a discretized Brillouin zone,[37] the latter of which is efficient and converges on a relatively modest k-mesh.

As an example we set the coupling strength t' to unity and on-site energy of the d orbital fixed at 30. When Δ is so large that two s and s' bands are well separated from each other (i.e. two copies of Hofstadter spectrum without overlap), the spectrum at $\alpha = \frac{p}{q}$ splits into $2q$ subbands. The Chern number of each subband can be found via the Diophantine equation. For example, at $\alpha = \frac{1}{3}$, there are 6 subbands and the Chern numbers for the lowest to the highest bands are 1, -2, 1, 1, -2, 1. The net Chern number depends on band filling, viz. it can change from zero to nonzero with band filling. When the on-site energy difference vanishes, the spectrum at $\alpha = \frac{1}{3}$ again splits into six bands but the corresponding Chern numbers become 4, -2, -2, -2, -2, and 4.

V. SUMMARY

In this paper the electronic, magnetic, and topological properties of particle-hole symmetry-broken semi-Dirac dispersion have been studied with the coupling strength t' between s (s') and d orbital as a generator of particle-hole asymmetry. When t' is zero, s and s' bands have the well known cosine dispersion on a square lattice and its spectrum contains a van Hove singularity at zero energy. As t' increases the density of states peak splits, separated by a dip as the lower band approaches zero energy. The upper band retains a divergent peak as a result of the flat region near the X point and the flat contour $\mathcal{C}$, while the lower peak has its origin from the saddle point somewhere along $\Gamma - X$. The touching points of upper and lower bands are the semi-Dirac points and lie on $\mathcal{C}$. The very different Fermi surfaces for electronic and hole doping have been presented and discussed. More general low energy dispersion than those for conventional zero gap semiconductors, Dirac points, and semi-Dirac points has been studied, and the criterion for a topological diabolical point for different types of low energy dispersion has been obtained.

The magnetic behavior of semi-Dirac fermions has been discussed via their Hofstadter spectrum, viz. the fractal energy level structure versus the fraction of flux quantum threading the unit cell. When t' is zero, the Hofstadter spectrum consists of two identical copies of the original Hofstadter spectrum. As the interaction strength is switched on, particle-hole symmetry is broken and new gaps emerge and grow near zero energy as well as in other regions. The opening of new gaps provides opportunities for tuning materials with engineered quantum Hall conductivity σ_{xy}. In light of recent studies of the Hofstadter spectrum of graphene (Dirac dispersion)[38] and the experimental observation of the Hofstadter spectrum on a Moiré lattice[39] and van der Waals heterostructure,[40] the Hofstadter spectrum of semi-Dirac systems could become of interest for experimental study.

VI. ACKNOWLEDGMENT

The calculations used resources of the National Energy Research Scientific Computing Center (NERSC), a DOE Office of Science User Facility supported by the Office of Science of the U.S. Department of Energy under Contract No. DE-AC02-05CH11231. Y. Quan acknowledges financial support from Beijing Normal University. W.E.P. was supported by the NSF grant DMR-1534719 under the DMREF program.

[1] M. Z. Hasan and C. Kane, Colloquium: Topological insulators, Rev. Mod. Phys. **82**, 3045 (2010).

[2] J. C. Smith, S. Banerjee, V. Pardo, and W. E. Pickett, Dirac point degenerate with massive bands at a topological quantum critical point, Phys. Rev. Lett. **106**, 056401 (2011).

[3] V. Pardo, J. C. Smith, and W. E. Pickett, Linear bands, zero-momentum Weyl semimetal, and topological transition in skutterudite-structure pnictides, Phys. Rev. B **85**, 214531 (2012).

[4] B. P. Neal, E. R. Ylvisaker, and W. E. Pickett, Quantum criticality in $NbFe_2$ induced by zero carrier velocity, Phys. Rev. B **84**, 085133 (2011).
[5] A. H. Castro Neto, F. Guinea, N. M. R. Peres, K. S. Novoselov, and A. K. Geim, The electronic properties of graphene, Rev. Mod. Phys. **81**, 109 (2009).
[6] D.N. Basov, M.M. Fogler, A. Lanzara, F. Wang, and Y. Zhang, Graphene spectroscopy, Rev. Mod. Phys. **86**, 959 (2014).
[7] I. M. Tsidilkovski, *Gapless Semiconductors* (Akademie-Verlag Berlin, Berlin, 1988). See especially page 73.
[8] A. Rüegg, C. Mitra, A. A. Demkov, and G. A. Fiete, Electronic structure of $(LaNiO_3)_2/(LaAlO_3)_N$ heterostructures grown along [111], Phys. Rev. B **85**, 245131 (2012).
[9] J. von Neumann and E. P. Wigner, On the behavior of eigenvalues in adiabatic processes, Physik. Z. **30**, 467 (1929). Translated in R. S. Knox and A. Gold, *Symmetry in the Solid State* (Benjamin, New York, 1964), p. 167.
[10] A. P. Schnyder, S. Ryu, A. Furusaki, and A. W. W. Ludwig, Classification of topological insulators and superconductors in three spatial dimensions, Phys. Rev. B **78**, 195125 (2008).
[11] T. T. Heikkilä and G. E. Volovik, Fermions with cubic and quartic spectrum, JETP Lett. **92**, 681 (2010).
[12] W. C. Herring, Accidental Degeneracy in the Energy Bands of Crystals, Phys. Rev. **52**, 365 (1937).
[13] W. C. Herring, On energy coincidences in the theory of Brillouin zones (Lancaster Press, Lancaster, PA, 1937). PhD thesis.
[14] P. B. Allen, What happens to geometric phase when spin-orbit interactions lift band degeneracies? arXiv:0709.1457 (2007).
[15] A. A. Burkov, M. D. Hook, and L. Balents, Topological nodal semimetals, Phys. Rev. B **84**, 235126 (2011).
[16] M. V. Berry, Aspects of degeneracy, in *Chaotic Behavior in Quantum Systems*, ed. G. Casatil (Plenum, New York, 1985), pp. 123-140.
[17] Y. Hasegawa, R. Konno, H. Nakano, and M. Kohmoto, Zero modes of tight-binding electrons on the honeycomb lattice, Phys. Rev. B **74**, 033413 (2006).
[18] P. Dietl, F. Piéchon, and G. Montambaux, New magnetic field dependence of Landau Levels in a Graphenelike Structure, Phys. Rev. Lett. **100**, 236405 (2008).
[19] G. Montambaux, G. Piéchon, J.-N. Fuchs, and M. O. Goerbig, Merging of Dirac points in a two-dimensional crystal, Phys. Rev. B **80**, 153412 (2009).
[20] P. Delplace and G. Montambaux, Semi-Dirac point in the Hofstadter spectrum, Phys. Rev. B **82**, 035438 (2010).
[21] V. Pardo and W. E. Pickett, Half-metallic semiDirac Point Generated by Quantum Confinement in TiO_2/VO_2 Nanostructures, Phys. Rev. Lett. **102**, 166803 (2009).
[22] S. Banerjee, R. R. P. Singh, V. Pardo, and W. E. Pickett, Tight-binding Modeling and Low-energy Behavior of the semi-Dirac Point, Phys. Rev. Lett. **103**, 016402 (2009).
[23] V. Pardo and W. E. Pickett, Metal-insulator Transition Through a semi-Dirac Point in Oxide Nanostructures: VO_2 (001) Layers Confined within TiO_2, Phys. Rev. B **81**, 035111 (2010).
[24] S. Banerjee and W. E. Pickett, Phenomenology of a semi-Dirac semi-Weyl semimetal, Phys. Rev. B **86**, 075124 (2012).
[25] H. Tasaki, From Nagaoka's Ferromagnetism to Flat-Band Ferromagnetism and Beyond: An Introduction to Ferromagnetism in the Hubbard Model, Prog. Theor. Phys. **99**, 489 (1998).
[26] Z. Liu, Z.-F. Wang, J.-W. Mei, Y.-S. Wu, and F. Liu, Flat Chern Band in a Two-Dimensional Organometallic Framework, Phys. Rev. Lett. **110**, 106804 (2013).
[27] R Takahashi and S. Murakami, Completely flat bands and fully localized states on surfaces of anisotropic diamond-lattice models, Phys. Rev. B **88**, 235303 (2013).
[28] F. Wang and Y. Ran, Nearly flat band with Chern number C=2 on the dice lattice, Phys. Rev. B **84**, 241103(R) (2011).
[29] D. R. Hofstadter, Energy levels and wavefunctions of Bloch electrons in rational and irrational magnetic fields, Phys. Rev. B **14** 2239 (1976).
[30] H. Huang, Z. Liu, H. Zhang, and D. Vanderbilt, Emergence of a Chern-insulating state from a semi-Dirac dispersion, Phys. Rev. B **92**, 161115 (2015).
[31] R. de Gail, M.-N. Fuchs, M. O. Goerbig, F. Piéchon, and G. Montambaux, Manipulation of Dirac points in graphene-like crystals, Physica B **407**, 1948 (2012).
[32] Q. Xu, R. Yu, Z. Fang, X. Dai, and H. Weng, Topological nodal line semimetals in the CaP_3 family of materials, Phys. Rev. B **95**, 045136 (2017).
[33] See for example G. H. Golub and C. F. Van Loan, *Matrix Computation*, 2nd Ed. (Johns Hopkins University Press, Baltimore, 1989).
[34] D. J. Thouless, M. Kohmoto, M. P. Nightingale, and M. den Nijs, Quantized Hall conductance in a two-dimensional periodic potential, Phys. Rev. Lett. **49**, 405 (1982).
[35] N. Goldman, Characterizing the Hofstadter butterfly's outline with Chern numbers, J. Phys. B **42**, 055302 (2009).
[36] G. Naumis and I. I. Satija, Topological Map of the Hofstadter Butterfly and van Hove Singularities, arXiv:1507.08130.
[37] T. Fukui, Y. Hatsugai, and H. Suzuki, Chern Numbers in Discretized Brillouin Zone: Efficient Method of Computing (Spin) Hall Conductances, J. Phys. Soc. Jpn. **74**, 1674 (2005).
[38] G. L. Yu, R. V. Gorbachev, J. S. Tu, A. V. Kretinin, Y. Cao, R. Jalil, F. Withers, L. A. Ponomarenko, B. A. Piot, M. Potemski, D. C. Elias, X. Chen, K. Watanabe, T. Taniguchi, I. V. Grigorieva, K. S. Novoselov, V. I. Fal'ko, A. K. Geim, A. Mishchenko, Hierarchy of Hofstadter states and replica quantum Hall ferromagnetism in graphene superlattices, Nat. Phys. **10**, 525529 (2014).
[39] C. R. Dean, L. Wang, P. Maher, C. Forsythe, F. Ghahari, Y. Gao, J. Katoch, M. Ishigami, P. Moon, M. Koshino, T. Taniguchi, K. Watanabe, K. L. Shepard, J. Hone, P. Kim, Hofstadter's butterfly and the fractal quantum Hall effect in Moiré superlattices, Nature **497**, 598 (2013).
[40] B. Hunt, J. D. Sanchez-Yamagishi, A. F. Young, M. Yankowitz, B. J. LeRoy, K. Watanabe, T. Taniguchi, P. Moon, M. Koshino, P. Jarillo-Herrero, R. C. Ashoori, Massive Dirac fermions and Hofstadter butterfly in a van der Waals heterostructure, Science **340**, 1427 (2013).